

Article

Simultaneous Viscosity Measurement of Suspended Blood and Plasma Separated by an Ultrasonic Transducer

Yang Jun Kang 

Department of Mechanical Engineering, Chosun University, 309 Pilmun-daero, Dong-gu, Gwangju 61452, Republic of Korea; yjkang2011@chosun.ac.kr; Tel.: +82-62-230-7052; Fax: +82-62-230-7055

Abstract: Blood viscosity is influenced by several factors, including red blood cell (RBC) deformability, hematocrit (Hct), and plasma protein levels. To effectively isolate the individual contributions of several factors, it is necessary to simultaneously measure the viscosities of the blood and plasma. In this study, the viscosities of suspended blood and plasma were obtained sequentially by adopting an ultrasonic transducer for plasma separation and a co-flowing microfluidic channel for viscosity measurement. To improve the measurement accuracy of viscosity, the correction factor was obtained through experiments and numerical simulations, which was then inserted into the analytical expression for viscosity. To stabilize the pulsatile blood flow resulting from a micropump, the frequency (f) and voltage (v) were set to $f = 300$ Hz and $v = 140$ au, respectively. Flexible polyethylene tubing (i.d. = 500 μm , length = 40 mm) was connected to the microfluidic device as an air damper. Consequently, the coefficient of variance of the blood velocity decreased by up to 1%. As a demonstration, suspended blood (Hct = 20%, 30%, and 40%) was prepared by adding normal RBCs to autologous plasma. Compared with the previous method, the present method overestimates the viscosity values of both the fluids (i.e., suspended blood: 14–25% and plasma: 7–21%). The present method has the ability to sequentially measure the viscosities of suspended blood and plasma. The integrated system contributes to reducing blood-handling procedures (i.e., blood collection, blood loading into the syringe, and syringe installation into the syringe pump).

Keywords: blood viscosity; plasma separation; microfluidic device; ultrasonic transducer; co-flowing method



Citation: Kang, Y.J. Simultaneous Viscosity Measurement of Suspended Blood and Plasma Separated by an Ultrasonic Transducer. *Appl. Sci.* **2023**, *13*, 3574. <https://doi.org/10.3390/app13063574>

Academic Editor: Gabriele Cervino

Received: 12 January 2023

Revised: 7 March 2023

Accepted: 9 March 2023

Published: 10 March 2023



Copyright: © 2023 by the author. Licensee MDPI, Basel, Switzerland. This article is an open access article distributed under the terms and conditions of the Creative Commons Attribution (CC BY) license (<https://creativecommons.org/licenses/by/4.0/>).

1. Introduction

Blood consists of cells (i.e., red blood cells, white blood cells, and platelets) and plasma [1]. Red blood cells (RBCs) play a critical role in gas (i.e., oxygen or carbon dioxide) transport between capillary vessels and peripheral tissues. As RBCs constitute approximately 40–50% of the blood volume, they have been regarded as a determinant factor of blood viscosity in comparison with the remaining cells. In other words, blood viscosity is predominantly determined by RBC mechanical phenotypes or hematocrit (Hct). Several biomechanical factors, including liquid-bilayer viscoelasticity, cytoplasmic viscosity, and apparent RBC morphology, contribute to changing blood viscosity [2]. However, Hct causes a substantial increase in blood viscosity [3]. Blood viscosity has a considerable influence on the blood flow in microcirculation or pressure drop within a confined vessel. In addition to RBCs, plasma contributes to elevated blood viscosity. According to previous studies, blood viscosity provides meaningful information for the monitoring or diagnosing of several diseases [4–6]. Recently, blood viscosity has been used to detect hyper-viscosity syndrome [7], blood coagulation [8,9], and RBC storage lesions [6,10].

A microfluidic platform has distinctive advantages, such as small sample consumption, short experiment time, fast response, and high sensitivity, when compared with bulk-sized conventional facilities. Several methodologies have been suggested for obtain blood viscosity [11]. Based on the well-known Poiseuille equation (i.e., pressure drop = fluidic

resistance \times flow rate) [12], fluidic resistance can be obtained by measuring either the pressure drop or flow rate. Fluidic resistance is proportional to the blood viscosity in a rectangular microfluidic channel. In principle, the blood viscosity can be obtained by measuring the fluidic resistance quantitatively, especially under a specific flow rate or pressure drop. According to previous studies, several methodologies for measuring fluidic resistance (i.e., interface location in the co-flowing channel [13,14], digital flow compartment [15–17], and droplet length [8,9]) or pressure drop (i.e., liquid-air interface movement [18], and membrane displacement [19–21]) have been suggested for obtaining blood viscosity. By supplying blood (or plasma) into a microfluidic channel, these methods are employed to measure the viscosity of blood or plasma. As the viscosity of whole (or suspended) blood is influenced by several factors, including RBC deformability, Hct, and plasma proteins, the contributions of several factors need to be understood. Therefore, it is necessary to isolate the individual effects of these factors. However, most of the previous methods focused on the accurate measurement of blood viscosity in microfluidic devices; they have a limitation in the simultaneous measurement of viscosities of whole blood (or suspended) blood and plasma. To resolve this issue, it is essential to separate the plasma from blood [22–24] and sequentially supply both fluids into a microfluidic device. Subsequently, the viscosities of both fluids were measured by adopting a coflowing method reported in previous studies [13,25–28]. Here, when blood and reference fluid are supplied at a specific flow rate ratio, interface between two fluids is determined by viscosity ratio of two fluids. As viscosity of reference fluid is specified in advance, blood viscosity can be obtained by quantifying blood-filled width in the coflowing channel.

In this study, the viscosity values of suspended blood and plasma were sequentially measured by adopting an ultrasonic transducer and co-flowing method in a microfluidic device. To measure the two viscosity values of both fluids sequentially, first, without operation of the ultrasonic transducer, a micropump was used to supply the suspended blood into the microfluidic device from the transducer. Blood viscosity was measured using the co-flowing technique. Second, by operating the ultrasonic transducer for a certain time, plasma and RBC were separated inside the transducer. Thereafter, the micropump was used to supply plasma into the microfluidic device from the transducer. The plasma viscosity was then obtained using the co-flowing method.

Compared with the previous study [22], using a micropump for delivering suspended blood and plasma separated by the ultrasonic chamber, the present method is capable of sequentially measuring the viscosities of blood and plasma. Moreover, the integrated system contributes to the reduction of blood handling procedures (i.e., blood collection from the ultrasonic chamber, blood loading into a disposable syringe, and blood delivery with a syringe pump). The expensive and bulky syringe pump was replaced with a micropump system.

2. Materials and Methods

2.1. Experimental Setup for Plasma Separation and Viscosity Measurement

To separate the plasma from the suspended blood and sequentially measure the individual viscosities of blood and plasma, as shown in Figure 1A, plasma separation and quantification of blood flow were suggested. Figure 1(A-i) shows a schematic of the experimental setup, including a microfluidic device, ultrasonic transducer, two pumps (i.e., micro pump for blood and syringe pump for reference fluid), and microscopic image acquisition system. The microfluidic device was composed of two inlets (a, b), a blood channel (BC, width = 200 μm), a reference fluid channel (RC, width = 200 μm), a co-flowing channel (CC, width = 400 μm), and an outlet. The depth of all the channels was fixed at 50 μm . Based on the protocol reported in a previous study [22], a polydimethylsiloxane (Sylgard 184, Dow Corning, Midland, MI, USA) microfluidic device was fabricated using the soft lithography technique. To stabilize the pulsatile blood flows generated by the micropump, an air damper was connected to inlet (a) [29]. The air damper was embodied by clamping the open end of polyethylene tubing (i.d. = 500 μm , length = L_t) with a steel pin. An ultrasonic transducer was used to separate the plasma from the suspended blood.

By turning on an ultrasonic transducer, the primary radiation force contributes to moving disaggregated RBCs to nodes or anti-nodes of pressure fields depending on sign of acoustic correction factor (i.e., $\phi > 0$: node, $\phi < 0$: anti-node). Next, secondary radiation force and Bernoulli force induce to aggregate RBCs continuously. When gravity force of aggregated RBCs is greater than buoyant force, RBCs sedimentation begins. Plasma is then separated from the suspended blood inside the transducer [22]. Based on a previous study [22], frequency (f) and acoustic power (AP) were set to $f = 2.1$ MHz and $AP = 2$ watt, respectively. Suspended blood (~5 mL) was loaded into the ultrasonic chamber. A micropump (MP6, Bartels Mikrotechnik, Emil-Figge, Germany) was used to supply blood from the transducer to the inlet (a) of the microfluidic device. The flow rate of the micropump was adjusted by setting two parameters (frequency: f , voltage: v) on a controller (Quadkey, Bartels Mikrotechnik, Emil-Figge, Germany). According to the viscosity measurement technique using the co-flowing method [13,22], the viscosity and flow rate of the reference fluid should be specified in advance. Here, $1 \times$ PBS (Phosphate-Buffered Saline) was selected as the reference fluid, and the flow rate was set to 1 mL/h using a syringe pump (neMESYS, Cetoni GmbH, Korbußen, Germany). The microfluidic device was mounted on an inverted optical microscope (IX53, Olympus, Shinjuku, Tokyo, Japan) equipped with a $10\times$ objective lens (N.A. = 0.25). To quantify the blood flow in the blood channel, microscopic images were captured using a high-speed camera (FASTCAM MINI, Photron, Tokyo, Japan). It was set to 5000 frames per second, and two microscopic images were sequentially captured, with an external trigger, at intervals of 1 s during all the experiments. Figure 1(A-ii) shows plasma separation within the ultrasonic transducer. Suspended blood was prepared by adding normal red blood cells (RBCs) to autologous plasma, and the Hct was set to 50%. As the ultrasonic standing wave contributed to accelerating RBC sedimentation in the transducer, the plasma volume (or height) increased significantly with time (i.e., $t_1 = t_0$, $t_2 = t_0 + 10$ min, $t_3 = t_0 + 10$ min, and $t_4 = t_0 + 10$ min).

2.2. Acquisition of Blood Velocity, Image Intensity, and Interface

As shown in Figure 1(A-iii), the blood velocity in the blood channel and interface in the co-flowing channel were obtained by digital image processing using MATLAB 2022a (Mathworks, Natick, MA, USA). First, a specific region of interest (ROI; $200 \mu\text{m} \times 550 \mu\text{m}$) was selected within the blood channel, and blood velocity fields were obtained using time-resolved micro-particle image velocimetry (micro-PIV) [30]. The interrogation window was set to $64 \text{ pixel} \times 64 \text{ pixel}$; one pixel corresponded to $3.3 \mu\text{m}$. The window overlap was set to 75%. Based on the analytical formula suggested in a previous study [31], the depth of correlation (DOC) was estimated to be $64.1 \mu\text{m}$. As the DOC was larger than the channel depth ($h = 50 \mu\text{m}$), it was assumed that the velocity fields remained unchanged along the channel depth. The blood velocity (U_b) was obtained by arithmetically averaging the velocity fields distributed over the ROI. The blood flow rate was then estimated as $Q_b = U_b \times A_c$, where A_c denotes the cross-sectional area of the rectangular channel (i.e., $A_c = \text{width} \times \text{depth}$). Additionally, based on the same ROI in the blood channel, the image intensity of the blood flow was obtained as I_b . Finally, to obtain the interface in the co-flowing channel, a specific ROI ($400 \mu\text{m} \times 550 \mu\text{m}$) was selected downstream from the junction area of the two streams. A grayscale image was converted into a binary image using the Otsu method [32]. The blood-filled width (w_b) was obtained by averaging variations in the blood-filled width within the ROI. The interface (α_b) was then obtained as $\alpha_b = w_b/w$.

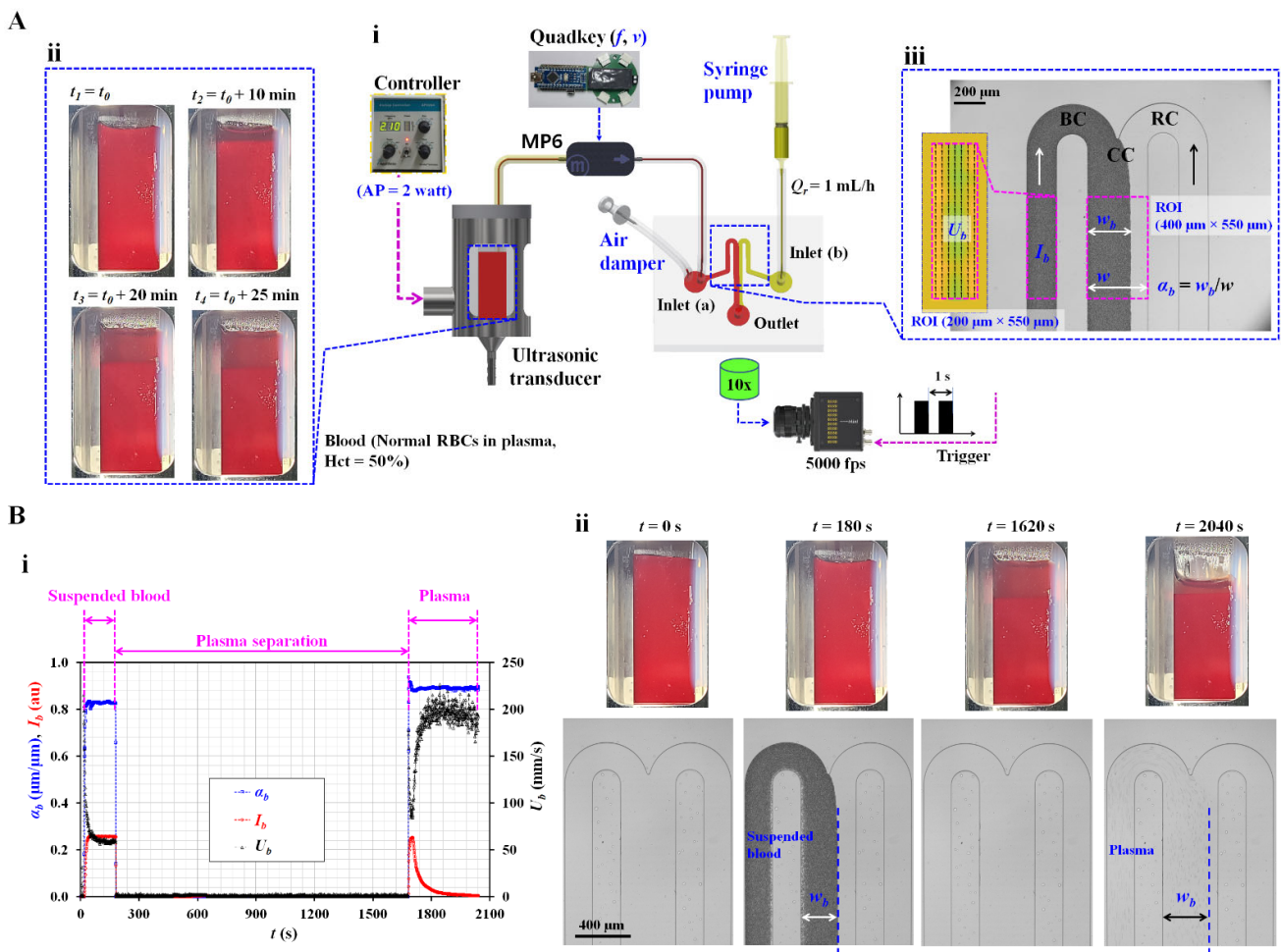


Figure 1. Proposed method for separating plasma and sequentially measuring individual viscosities of blood and plasma. (A) Experimental setup, plasma separation, and quantification of blood. (i) Schematic of the experimental setup, including, a microfluidic device, an ultrasonic transducer, two pumps (i.e., micro pump and syringe pump), and an image acquisition system. (ii) Plasma separation from the suspended blood with an elapse of time (i.e., $t_1 = t_0$, $t_2 = t_0 + 10$ min, $t_3 = t_0 + 10$ min, and $t_4 = t_0 + 10$ min). (iii) Quantification of blood velocity (U_b) and interface (α_b). (B) Quantification of three parameters (i.e., interface, image intensity, and blood velocity) for suspended blood (i.e., normal RBCs suspended in plasma, and Hct = 50%). (i) Temporal variations of α_b , I_b , and U_b . First, the suspended blood was supplied for 3 min. Next, plasma was separated from the blood for 25 min; plasma was then supplied for 6 min. (ii) Snapshots of the ultrasonic chamber and microscopic images with respect to time (t) ($t = 0, 180, 1620,$ and 2040 s).

2.3. Operational Protocol of the Present Method

To measure the individual viscosities of suspended blood and plasma, Figure 1(B-i) represents temporal variations of the three parameters (i.e., U_b , I_b , and α_b) obtained through the overall operational protocols suggested in the present study. U_b and α_b were used to obtain the viscosity values of each fluid; I_b was used to detect the specific time when the suspended blood or plasma flowed in the blood channel or co-flowing channel. Suspended blood (Hct = 50%) was prepared by adding normal RBCs to plasma. First, to measure its viscosity, the suspended blood was supplied continuously into the microfluidic device with a micropump (i.e., $t < 180$ s). Here, the frequency and voltage were set to $f = 300$ Hz and $v = 140$ au, respectively. The micropump was then turned off, and the ultrasonic transducer was turned on to separate plasma from the blood (180 s $<$ $t <$ 1680 s). Finally, the transducer was turned off. The plasma was supplied to the microfluidic device by turning on the micropump. Figure 1(B-ii) shows snapshots of the ultrasonic chamber and

microscopic images with respect to time (t) ($t = 0, 180, 1620, \text{ and } 2040$ s). Before $t = 180$ s, suspended blood was supplied and loaded into the microfluidic device. The co-flowing channel was partially filled with blood and $1 \times$ PBS, and the blood volume decreased in the ultrasonic transducer. Plasma separation continued at a specific time, ranging from $t = 180$ s to $t = 1680$ s. After the micropump was turned off, all the channels were filled with the reference fluid. At $t = 2040$ s, the plasma was loaded into the co-flowing channel. Based on the suggested operation protocol of the micropump and ultrasonic transducer, the three parameters were obtained, and further used to sequentially acquire the two viscosity values of the blood and plasma.

2.4. Preparation of Suspended Blood

Concentrated RBC Bags (~320 mL) were purchased from Gwangju–Chonnam Blood Bank (Gwangju, Republic of Korea). After the concentrated RBCs were sufficiently washed with $1 \times$ PBS, several types of suspended blood samples were prepared by adding normal RBCs to autologous plasma.

3. Results and Discussion

3.1. Quantification of the Correction Factor of Co-Flowing Method for Accurate Viscosity Measurement

In this study, the co-flowing method was used to sequentially measure the viscosities of both the blood and plasma. According to the previous method, the fluid viscosity can be obtained by detecting the interface in the co-flowing channel. However, the performance of the co-flowing method varies depending on the interfacial location [14]. A correction factor was suggested to minimize the measurement error. A previous study reported that the correction factor depends on the depth/width and interface [28]; that is, when a microfluidic channel is newly designed, a correction factor should be obtained via experiment or numerical simulation. Figure 2(A-i) shows the mathematical representation of the co-flowing channel in terms of two fluidic resistance elements. As the co-flowing channel was filled with blood (i.e., subscript 't') and reference fluid (i.e., subscript 'r'), frictional loss of each fluid was represented with fluidic resistance elements (i.e., R_t, R_r). At the outlet ('∇'), the pressure was set to zero (i.e., $P = 0$). Q_t and Q_r denote the flow rates of the blood and reference fluid, respectively. For a simple mathematical representation, the two fluid streams are represented as R_t and R_r . Both the fluidic resistance elements were connected in parallel. Based on the Poiseuille flow equation (i.e., $\Delta P = R \times Q$), the pressure of each fluid stream can be expressed as

$$P_r = \frac{12 \mu_r L}{(1 - \alpha_t) w h^3} \times Q_r \quad (1)$$

$$P_t = \frac{12 \mu_t L}{CF \alpha_t w h^3} \times Q_t \quad (2)$$

In Equation (2), the correction factor (CF), which depends on the interface (i.e., $CF = CF[\alpha_t]$), was added to compensate for the mathematical modeling error resulting from the approximation of a real physical problem [28]. As the two fluid streams were confined in straight and rectangular channels, both the streams had the same pressure at a distance (L) from the outlet.

Based on the same pressure condition (i.e., $P_t = P_r$), the viscosity of the test fluid was expressed as

$$\mu_t = \mu_r \times \left(\frac{Q_r}{Q_t} \right) \times \left(\frac{\alpha_t}{1 - \alpha_t} \right) \times CF(\alpha_t) \quad (3)$$

Here, the test fluid and reference fluid were selected as the plasma and $1 \times$ PBS, respectively. To simulate variations in α_t by means of a CFD Solver (CFD-ACE+, ESI Group, Paris, France), the viscosity ratio of the two fluids was given as $\mu_t/\mu_r = 1.674$. As shown in Figure 2(B-i), microscopic images representing α_t were summarized with

respect to $Q_r/Q_t = 1/0.2, 1/0.5, 1/1, 0.5/1, \text{ and } 0.2/1$. Additionally, based on the numerical simulation results, as shown in Figure 2(B-ii), the variations in α_t were clearly visualized with a binary color representation with respect to Q_t/Q_r . Consequently, α_t showed a tendency to increase at higher value of Q_t/Q_r . Both the methods provide consistent variations in α_t with respect to Q_r/Q_t . To obtain the variations in CF with respect to α_t , the analytical formula of the correction factor was derived as

$$CF(\alpha_t) = \left(\frac{\mu_t}{\mu_r}\right) \times \left(\frac{1 - \alpha_t}{\alpha_t}\right) \times \left(\frac{Q_t}{Q_r}\right) \tag{4}$$

Based on Equation (4), as shown in Figure 2C, variations in the correction factor were obtained as a function of the interface. The CF obtained from the numerical simulation was higher than that obtained from the experimental results. In this study, according to the linear regression analysis of the experimental results, the CF was best fitted as $CF = 0.7004 \alpha_t + 0.6216$ ($R^2 = 0.9469$). Therefore, by inserting the regression formula of CF into Equation (3), the viscosities of the blood and plasma were obtained with sufficient accuracy.

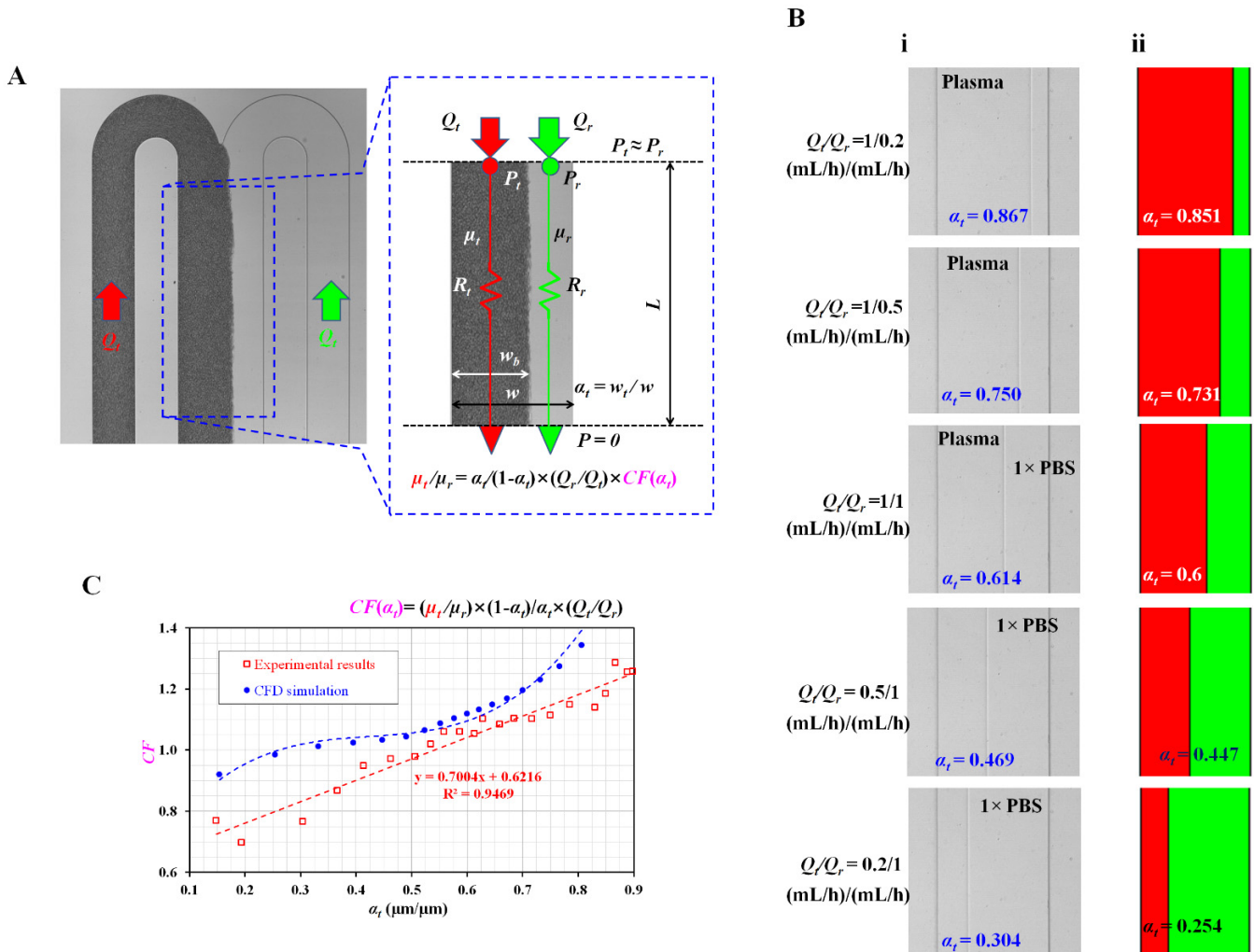


Figure 2. Derivation of blood viscosity formula in terms of fluidic circuit elements. (A) Mathematical representation of co-flowing channel. (B) Quantitative comparison between the experimental and numerical simulation results. (i) Experimental results showing variations of interface with respect to flow-rate ratio (Q_t/Q_r) ($Q_t/Q_r = 1/0.2, 1/0.5, 1/1, 0.5/1, \text{ and } 0.2/1$). (ii) Numerical simulation results showing variations of interface with respect to Q_t/Q_r . (C) Variations of CF obtained by experimental and numerical simulation results with respect to the interface. Based on linear regression analysis of the experimental results, the CF was best fitted as $CF = 0.7004 \alpha_t + 0.6216$ ($R^2 = 0.9469$).

3.2. Quantitative Evaluation of Blood Flow and Blood Flow Stabilization

A micropump delivered suspended blood using piezoelectric membrane vibration resulting in the periodic fluctuations in the blood flow [33]. However, to measure the shearing viscosity of the blood or plasma, it was essential to maintain a constant flow rate (or velocity) during the experiment. Therefore, the frequency of micropump was adjusted to reduce the fluctuations in blood flow. Additionally, the effect of the air damper on the stabilization of blood flow was evaluated by changing the length (or cavity) of the air damper. Suspended blood (Hct = 50%) was prepared by adding normal RBCs to autologous plasma.

To quantify the blood flow delivered by the micropump, the velocity (U_b) and interface (α_b) were monitored without the addition of an air damper. Figure 3A shows microscopic images of variations in the interface with respect to the operational frequency (f) ([i] $f = 100$ Hz, [ii] $f = 300$ Hz, [iii] $f = 400$ Hz, and [iv] $f = 800$ Hz). The excitation voltage of the micropump was fixed at $v = 140$ au, where au denotes an arbitrary unit. α_b showed a tendency to decrease at higher values of the operational frequency. Based on the microscopic images captured over time, temporal variations in U_b and I_b were obtained with respect to the operational frequency. Figure 3(B-i) shows the temporal variations in U_b with respect to f . At $f = 100$ Hz, U_b exhibited large alternating blood flow. However, when the frequency was shifted to 300 Hz, the fluctuations decreased substantially. From the results, it was inferred that the resonance frequency of the micropump was close to 100 Hz. To reduce fluctuations in the blood velocity, the operational frequency must be set above 100 Hz. Figure 3(B-ii) shows the variations in U_b and coefficient of variance (COV) (COV = standard deviation/mean) with respect to f . U_b showed a tendency to gradually decrease with respect to operation frequency. Additionally, the COV had a minimum value at $f = 300$ or 400 Hz. Figure 3(B-iii) shows the temporal variations in α_b with respect to f ; the value of α_b gradually decreased at higher frequencies. The fluctuation in α_b is very small with respect to f , which implies that it remained constant with respect to the operational frequency. Figure 3B-iv shows the variations in α_b and COV with respect to the operational frequency; α_b decreased linearly with respect to f , and the COV was less than 1%. From the results, it can be concluded that the blood velocity (U_b) was significantly influenced by the operational frequency when compared with the interface (α_b). Based on the experimental results, the operational requirement was set to $f = 300$ Hz during the subsequent experiments.

To reduce periodic fluctuations in the blood flow, an air damper was connected to inlet (a). To substantially increase the air compliance effect, the air cavity inside the air damper was adjusted by increasing the length of the polyethylene tubing (L_t). Figure 3(C-i) shows a schematic of the air damper connected to the inlet (a) of the microfluidic device. The flow rate of the reference fluid ($1 \times$ PBS) was set to 1 mL/h using a syringe pump. The control parameters of the micropump were set to $f = 300$ Hz and $v = 140$ au. Figure 3(C-ii) shows the temporal variations in U_b with respect to $L_t = 0, 20, 40,$ and 60 mm. The air damper contributed to the decrease in periodic fluctuations of U_b . Figure 3(C-iii) shows the variations in CV with respect to L_t ; CV decreased significantly from 3% to 1% with the addition of the air damper. From the results, the length of the air damper was set as $L_t = 40$ mm during the subsequent experiments.

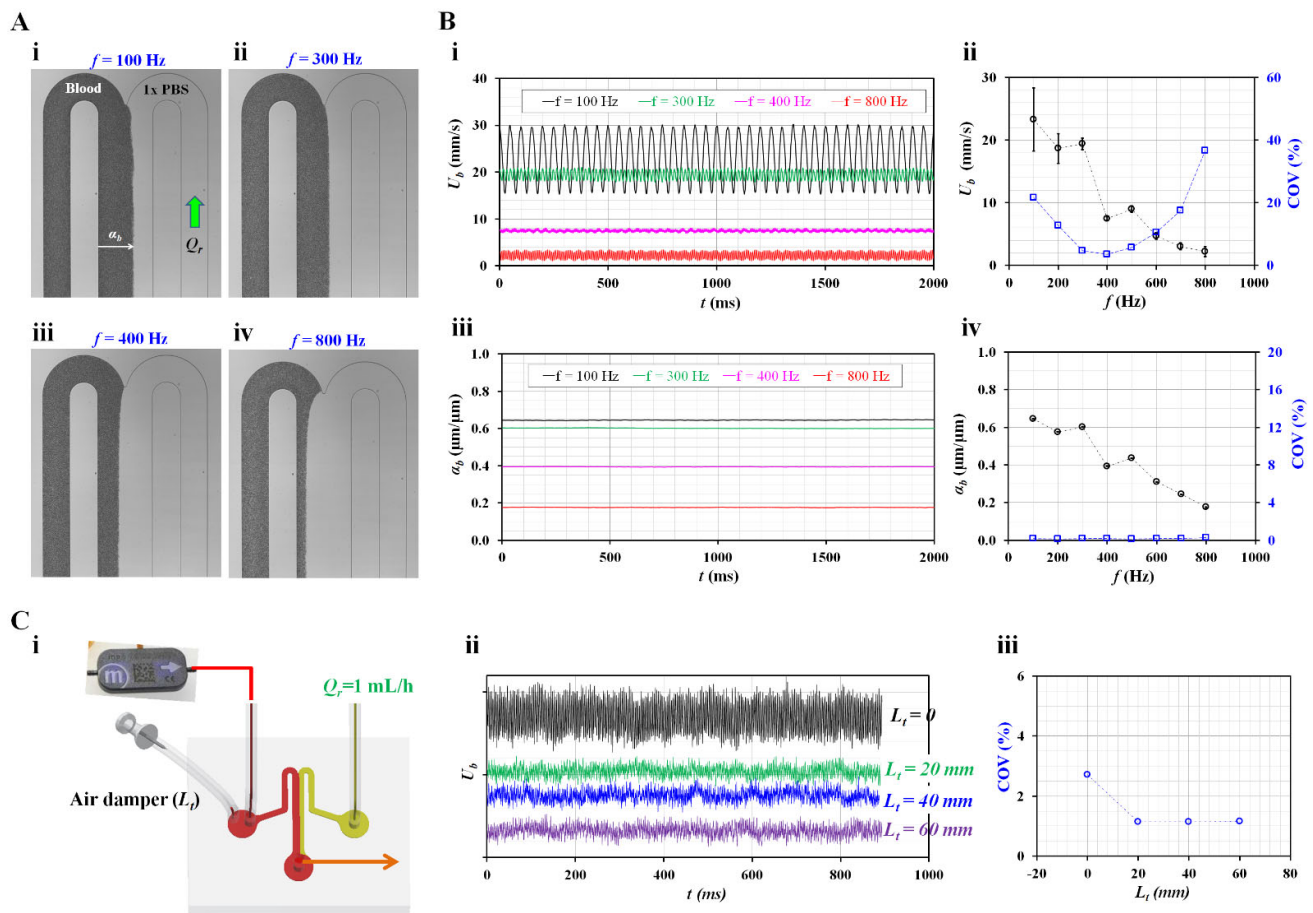


Figure 3. Quantitative evaluation of blood flow delivered by micro pump and blood flow stabilization with air damper. (A) Microscopic images showing variations of interface with respect to operational frequency (f) ([i] $f = 100 \text{ Hz}$, [ii] $f = 300 \text{ Hz}$, [iii] $f = 400 \text{ Hz}$, and [iv] $f = 800 \text{ Hz}$). (B) Contributions of operational frequency to blood velocity and interface. (i) Temporal variations of U_b with respect to f . (ii) Variations of U_b and COV with respect to f . (iii) Temporal variations of α_b with respect to f . (iv) Variations of α_b and COV with respect to f . (C) Contribution of air damper to blood flow stabilization. (i) Schematic diagram showing air damper connected to a microfluidic device. (ii) Temporal variations of U_b with respect to $L_t = 0, 20, 40,$ and 60 mm . (iii) Variations of CV with respect to L_t .

3.3. Simultaneous Viscosity Measurement of suspended Blood and Plasma with Respect to Hematocrit

To date, the contributions of vital factors have been quantitatively evaluated in terms of blood velocity or interface. As a demonstration, the proposed method was applied to measure the viscosities of suspended blood and plasma. Suspended blood (Hct = 20, 30, and 40%) was prepared by adding normal RBCs to the same autologous plasma. This was intended to detect the contribution of Hct in blood viscosity as the suspended blood was prepared using the same diluent.

Based on the operational protocol suggested in the present study, as shown in Figure 4A, temporal variations in α_b , I_b , and U_b were obtained with respect to Hct ([i] Hct = 20%, [ii] Hct = 30%, and [iii] Hct = 40%). Considering the suspended blood, U_b tended to decrease at higher Hct values. The Hct contributed to the increase in α_b and I_b . The time elapsed for separating plasma from the suspended blood increased at higher Hct values. When the micropump was turned on, α_b immediately reached a steady state. However, U_b took a considerable amount of time to arrive at a steady value. It was inferred that the air damper contributed to the increase in the time delay of U_b rather than that of α_b .

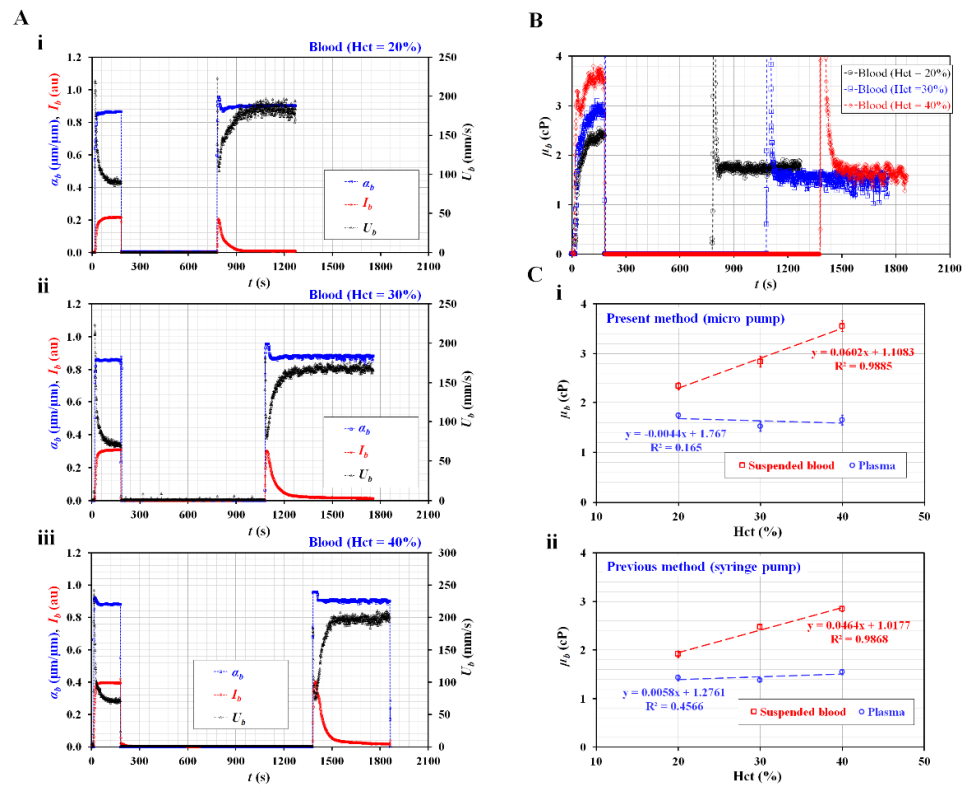


Figure 4. Sequential viscosity measurement of suspended blood and plasma with respect to Hct. (A) Temporal variations of α_b , I_b , and U_b with respect to Hct = 20%, 30%, and 40%. (B) Temporal variations of μ_b with respect to Hct. (C) Quantitative comparison between the present method (i.e., blood delivery with micro pump) and previous method (i.e., blood delivery with syringe pump). (i) Steady viscosity value of blood and plasma obtained using the present method with respect to Hct. (ii) Viscosity value of blood and plasma obtained by previous method with respect to Hct.

Based on the temporal variations of α_b and U_b , the individual viscosities of the suspended blood and plasma were obtained using Equation (3). As shown in Figure 4B, temporal variations in μ_b were observed with respect to Hct. Owing to the dynamic delay resulting from the air damper, μ_b of suspended blood reached a steady value after approximately 120 s. Blood viscosity tended to increase at higher values of Hct. The μ_b of the plasma reached a steady value within 60 s. According to a previous study, the time constant (i.e., time delay) is influenced by fluidic resistance and compliance (i.e., time constant = fluidic resistance \times compliance) [30,34]. The time delay of suspended blood was longer than that of plasma because the viscosity of blood was higher than that of plasma. There was no significant difference in the viscosities of the plasma separated from each suspended blood sample. Figure 4C shows a quantitative comparison between the proposed method (i.e., blood delivery with a micropump) and previous method (i.e., blood delivery with a syringe pump). In the present method, the individual viscosities of suspended blood and plasma were obtained as the mean \pm standard deviation after the viscosity reached a steady value. However, in the previous method, to measure viscosity of suspended blood, the suspended blood was loaded into disposable syringe and installed in the syringe pump; the blood flow rate was set at 1 mL/h. As the shear rate of the blood flow was estimated to be greater than 1000 s^{-1} , it was assumed that the blood behaved as a Newtonian fluid. Next, to measure the viscosity of the plasma, it was collected from the ultrasonic transducer, as shown in Figure 1(A-ii). The plasma was loaded into a disposable syringe. After the syringe was installed in the syringe pump, the flow rate of the plasma was set to 1 mL/h. In contrast with the previous method, the present method did not require the loading of blood into a disposable syringe, and the syringe pump was replaced with a micropump. Figure 4(C-i) shows the steady viscosity values of blood and plasma

obtained by the present method with respect to Hct. In addition, Figure 4(C-ii) shows the viscosity values of the blood and plasma obtained by the previous method with respect to Hct. As expected, the blood viscosity tended to increase linearly with respect to Hct ($R^2 = 0.98$); the plasma viscosity remained constant ($R^2 = 0.17$ – 0.46). The present method overestimated the viscosity values of both the fluids by approximately 14–25% (for suspended blood) and 7–21% (for plasma) when compared with the previous method. The two methods only had differences in blood delivery (i.e., previous method: syringe pump, and present method: micro pump). According to a previous study [35], blood velocity is substantially influenced by Hct. Therefore, it is inferred that the blood flow rate was underestimated by the micro-PIV technique. Additionally, with respect to the suspended blood, the delivery time must be increased to guarantee a steady range of U_b .

From the experimental results, it was concluded that the present method has the ability to sequentially measure the viscosities of suspended blood and plasma. This method simplifies blood handling procedures (i.e., blood collection and loading), and the syringe pump is replaced with a micropump.

4. Conclusions

In this study, the viscosity values of the suspended blood and plasma were sequentially measured using an ultrasonic transducer and a co-flowing method in a microfluidic device. As a suggested protocol, first, the suspended blood was supplied to the microfluidic device, and blood viscosity was measured using the co-flowing technique. Second, the plasma was separated from the suspended blood using an ultrasonic transducer. Third, the plasma viscosity was obtained by supplying plasma to the microfluidic device. To improve the measurement accuracy of the co-flowing method, the correction factor was calculated by conducting experiments and numerical simulations. Based on the quantitative studies of vital parameters, the control parameters (i.e., frequency and voltage) of the micropump were set to $f = 300$ Hz and $v = 140$ au, respectively. Additionally, by adopting an air damper (i.d. = 500 μm , length = 40 mm), the COV of the blood velocity was improved to 1%. As a demonstration, suspended blood (Hct = 20%, 30%, and 40%) was prepared by adding normal RBCs to the same autologous plasma. According to the experimental results, blood viscosity tended to increase linearly within the hematocrit. The plasma viscosity remained constant because the suspended blood was prepared using the same diluent. Compared with the previous method (i.e., blood delivery), the present method (i.e., blood delivery with a micro pump) overestimated the viscosity values of both the fluids by approximately 14–25% (for suspended blood) and 7–21% (for plasma). Based on the analytical model, it was inferred that the underestimation of the blood velocity caused a difference in viscosity. In the future studies, it will be necessary to improve the quantification of blood velocity using the micro-PIV technique. Furthermore, the operation protocol of the micropump will be optimized to guarantee sufficient blood flow.

Funding: This work was supported by the Basic Science Research Program through the NRF, funded by the Ministry of Education (NRF-2021R1I1A3040338).

Institutional Review Board Statement: This study was conducted in accordance with the Declaration of Helsinki and approved by the ethical committee of Chosun University under reference code (2-1041055-AB-N-01-2022-47).

Informed Consent Statement: Not applicable.

Data Availability Statement: Not applicable.

Acknowledgments: The author would like to acknowledge So-Mi Kim and Si-Young Park, who helped the author conduct this study. In addition, the author would like to sincerely thank Sanghwa Jeong for allowing the use of an ultrasonic transducer.

Conflicts of Interest: The authors declare no conflict of interest.

References

1. Baskurt, O.K.; Meiselman, H.J. Blood rheology and hemodynamics. *Semin. Thromb. Hemost.* **2003**, *29*, 435–450. [[CrossRef](#)] [[PubMed](#)]
2. Trejo-Soto, C.; Lázaro, G.R.; Pagonabarraga, I.; Hernández-Machado, A. Microfluidics approach to the mechanical properties of red blood cell membrane and their effect on blood rheology. *Membranes* **2022**, *12*, 217. [[CrossRef](#)] [[PubMed](#)]
3. Kim, B.J.; Lee, Y.S.; Zhanov, A.; Yang, S. A physiometer for simultaneous measurement of whole blood viscosity and its determinants: Hematocrit and red blood cell deformability. *Analyst* **2019**, *144*, 3144–3157. [[CrossRef](#)] [[PubMed](#)]
4. Fornal, M.; Korbut, R.A.; Lekka, M.; Pyka-Fościk, G.; Wizner, B.; Styczen, J.; Grodzicki, T. Rheological properties of erythrocytes in patients with high risk of cardiovascular disease. *Clin. Hemorheol. Microcirc.* **2008**, *39*, 213–219. [[CrossRef](#)] [[PubMed](#)]
5. Lowe, G.D.; Drummond, M.M.; Lorimer, A.R.; Hutton, I.; Forbes, C.D.; Prentice, C.R.; Barbenel, J.C. Relation between extent of coronary artery disease and blood viscosity. *Br. Med. J.* **1980**, *280*, 673–674. [[CrossRef](#)]
6. Barshtein, G. Biochemical and biophysical properties of red blood cells in disease. *Biomolecules* **2022**, *12*, 923. [[CrossRef](#)]
7. Musick, J.O.; Fibben, K.S.; Lam, W.A. Hyperviscosity syndromes; hemorheology for physicians and the use of microfluidic devices. *Curr. Opin. Hematol.* **2022**, *29*, 290–296. [[CrossRef](#)]
8. Chen, L.; Li, D.; Liu, X.; Xie, Y.; Shan, J.; Huang, H.; Yu, X.; Chen, Y.; Zheng, W.; Li, Z. Point-of-Care Blood Coagulation Assay Based on Dynamic Monitoring of Blood Viscosity Using Droplet Microfluidics. *ACS Sensors* **2022**, *7*, 2170–2177. [[CrossRef](#)]
9. Mena, S.E.; Li, Y.; McCormick, J.; McCracken, B.; Colmenero, C.; Ward, K.; Burns, M.A. A droplet-based microfluidic viscometer for the measurement of blood coagulation. *Biomicrofluidics* **2020**, *14*, 014109. [[CrossRef](#)]
10. Park, J.H.; Go, T.; Lee, S.J. Label-Free Sensing and Classification of Old Stored Blood. *Ann. Biomed. Eng.* **2017**, *45*, 2563–2573. [[CrossRef](#)]
11. Kang, Y.J.; Lee, S.-J. In vitro and ex vivo measurement of the biophysical properties of blood using microfluidic platforms and animal models. *Analyst* **2018**, *143*, 2723–2749. [[CrossRef](#)]
12. Oh, K.W.; Lee, K.; Ahn, B.; Furlani, E.P. Design of pressure-driven microfluidic networks using electric circuit analogy. *Lab Chip* **2012**, *12*, 515–545. [[CrossRef](#)]
13. Kang, Y.J. Biosensing of Haemorheological Properties Using Microblood Flow Manipulation and Quantification. *Sensors* **2022**, *23*, 408. [[CrossRef](#)]
14. Hintermüller, M.A.; Offenzeller, C.; Jakoby, B. A microfluidic viscometer with capacitive readout using screen-printed electrodes. *IEEE Sens. J.* **2021**, *21*, 2565–2572. [[CrossRef](#)]
15. Kim, B.J.; Lee, S.Y.; Jee, S.; Atajanov, A.; Yang, S. Micro-viscometer for measuring shear-varying blood viscosity over a wide-ranging shear rate. *Sensors* **2017**, *17*, 1442. [[CrossRef](#)]
16. Kang, Y.J.; Yoon, S.Y.; Lee, K.-H.; Yang, S. A highly accurate and consistent microfluidic viscometer for continuous blood viscosity measurement. *Artif. Organs* **2010**, *34*, 944–949. [[CrossRef](#)]
17. Kang, Y.J.; Ryu, J.; Lee, S.-J. Label-free viscosity measurement of complex fluids using reversal flow switching manipulation in a microfluidic channel. *Biomicrofluidics* **2013**, *7*, 044106. [[CrossRef](#)]
18. Méndez-Mora, L.; Cabello-Fusarés, M.; Trejo-Soto, C.; Alarcón, T.; Ferré-Torres, J.; Riera-Llobet, C.; Hernandez-Machado, A. Microrheometer for biofluidic analysis: Electronic detection of the fluid-front advancement. *Micromachines* **2021**, *12*, 726. [[CrossRef](#)]
19. Liu, L.; Hu, D.; Lam, R.H.W. Microfluidic Viscometer Using a Suspending Micromembrane for Measurement of Biosamples. *Micromachines* **2020**, *11*, 934. [[CrossRef](#)]
20. Mustafa, A.; Eser, A.; Aksu, A.C.; Kiraz, A.; Tanyeri, M.; Erten, A.; Yalcin, O. A micropillar-based microfluidic viscometer for Newtonian and non-Newtonian fluids. *Anal. Chim. Acta* **2020**, *1135*, 107–115. [[CrossRef](#)]
21. Lee, T.A.; Liao, W.H.; Wu, Y.F.; Chen, Y.L.; Tung, Y.C. Electrofluidic Circuit-Based Microfluidic Viscometer for Analysis of Newtonian and Non-Newtonian Liquids under Different Temperatures. *Anal. Chem.* **2018**, *90*, 2317–2325. [[CrossRef](#)] [[PubMed](#)]
22. Kim, G.; Jeong, S.; Kang, Y.J. Ultrasound standing wave-based cell-to-liquid separation for measuring viscosity and aggregation of blood sample. *Sensors* **2020**, *20*, 2284. [[CrossRef](#)] [[PubMed](#)]
23. Cousins, C.M.; Holownia, P.; Hawkes, J.J.; Limaye, M.S.; Price, C.P.; Keay, P.J.; Coakley, W.T. Plasma preparation from whole blood using ultrasound. *Ultrasound Med. Biol.* **2000**, *26*, 881–888. [[CrossRef](#)] [[PubMed](#)]
24. Petersson, F.; Nilsson, A.; Holm, C.; Jönsson, H.; Laurell, T. Separation of lipids from blood utilizing ultrasonic standing waves in microfluidic channels. *Analyst* **2004**, *129*, 938–943. [[CrossRef](#)]
25. Kang, Y.J. Quantitative monitoring of dynamic blood flows using coflowing laminar streams in a sensorless approach. *App. Sci.* **2021**, *11*, 7260. [[CrossRef](#)]
26. Kang, Y.J. Blood viscoelasticity measurement using interface variations in coflowing streams under pulsatile blood flows. *Micromachines* **2020**, *11*, 245. [[CrossRef](#)]
27. Kang, Y.J. Periodic and simultaneous quantification of blood viscosity and red blood cell aggregation using a microfluidic platform under in-vitro closed-loop circulation. *Biomicrofluidics* **2018**, *12*, 024116. [[CrossRef](#)]
28. Kang, Y.J. Continuous and simultaneous measurement of the biophysical properties of blood in a microfluidic environment. *Analyst* **2016**, *141*, 6583–6597. [[CrossRef](#)]
29. Zhou, Y.; Liu, J.; Yan, J.; Zhu, T.; Guo, S.; Li, S.; Li, T. Standing air bubble-based micro-hydraulic capacitors for flow stabilization in syringe pump-driven systems. *Micromachines* **2020**, *11*, 396. [[CrossRef](#)]

30. Thielicke, W.; Stamhuis, E.J. PIVlab—Towards user-friendly, affordable and accurate digital particle image velocimetry in MATLAB. *J. Open Res. Softw.* **2014**, *2*, e30. [[CrossRef](#)]
31. Bourdon, C.J.; Olsen, M.G.; Gorby, A.D. The depth of correction in micro-PIV for high numerical aperture and immersion objectives. *J. Fluid Eng. T. ASME* **2006**, *128*, 883–886. [[CrossRef](#)]
32. Otsu, N. A threshold selection method from gray-level histograms. *IEEE Trans. Syst. Man. Cybern.* **1979**, *9*, 62–66. [[CrossRef](#)]
33. Kim, B.H.; Kim, I.C.; Kang, Y.J.; Ryu, J.; Lee, S.J. Effect of phase shift on optimal operation of serial-connected valveless micropumps. *Sens. Actuators A Phys.* **2014**, *209*, 133–139. [[CrossRef](#)]
34. Kang, Y.J. Experimental investigation of air compliance effect on measurement of mechanical properties of blood sample flowing in microfluidic channels. *Micromachines* **2020**, *11*, 460. [[CrossRef](#)]
35. Kang, Y.J. Microfluidic-based biosensor for blood viscosity and erythrocyte sedimentation rate using disposable fluid delivery system. *Micromachines* **2020**, *11*, 215. [[CrossRef](#)]

Disclaimer/Publisher’s Note: The statements, opinions and data contained in all publications are solely those of the individual author(s) and contributor(s) and not of MDPI and/or the editor(s). MDPI and/or the editor(s) disclaim responsibility for any injury to people or property resulting from any ideas, methods, instructions or products referred to in the content.